SSC-174

The Superconducting Super Collider

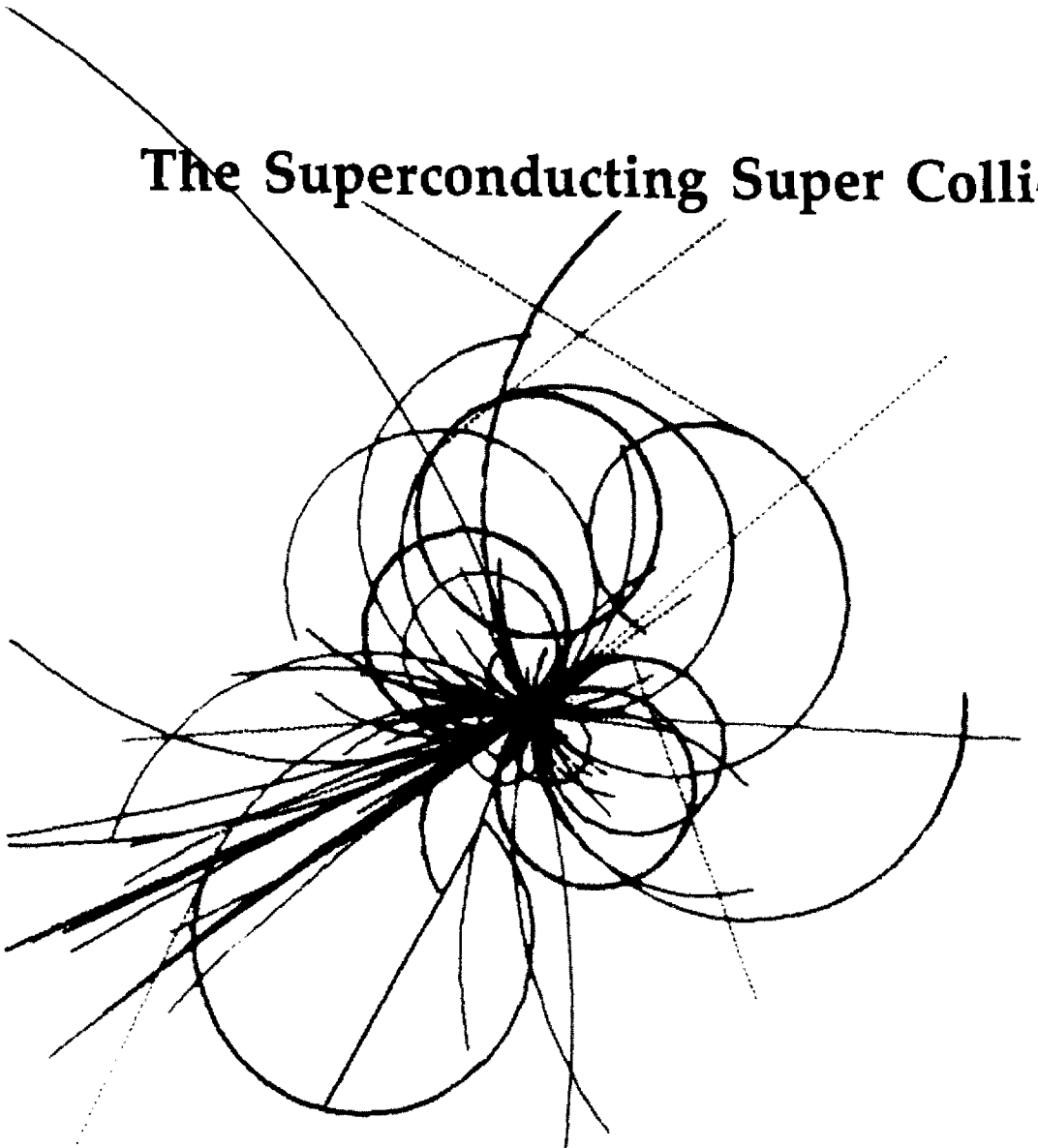

A Symplectic Model of Coherent Beam-Beam Quadrupole Modes

M.A. Furman
K.Y. Ng and A.W. Chao

SSC Central Design Group

April 1988

SSC-174

A SYMPLECTIC MODEL OF COHERENT BEAM-BEAM QUADRUPOLE MODES

M. A. Furman, K. Y. Ng, and A. W. Chao
SSC Central Design Group*

April 1988

*Operated by Universities Research Association for the U. S. Department of Energy

SSC-174

A SYMPLECTIC MODEL OF COHERENT BEAM-BEAM QUADRUPOLE MODES

M. A. Furman, K. Y. Ng and A. W. Chao
SSC Central Design Group
April 1988

ABSTRACT

We consider a simple model to study the effects of the beam-beam force on the dynamics of colliding beams. We focus on the quadrupole modes of the coherent oscillation. The ingredients are: (1) linearized beam-beam kicks, (2) damping and noise due to synchrotron radiation, and (3) linear transport between beam-beam kicks. The dynamical variables are the 2nd-order moments of the canonical variables q, p, which include the *rms* bunch size. Our model is self-consistent in the sense that no higher order moments are generated by the linearized beam-beam kicks, and that the only source of violation of symplecticity is the radiation. We discuss the cases of round and flat beams. Depending on the values of the tune and beam-beam kick strength, we observe states in which otherwise identical bunches have sizes that are equal, or unequal, or periodic, or behave chaotically from turn to turn. Possible implications of luminosity saturation with increasing beam intensity are discussed.

1. Introduction

The beam-beam interaction is widely recognized as an important factor in the performance of colliding beam storage rings. Among its possible effects are tune shifts, beam focusing at low current, beam blow-up at high current, saturation of the beam-beam parameter and luminosity, the "flip-flop" effect and its associated hysteresis.[1] Many studies have been done in the "weak-weak" and "strong-weak" limits, which involve a linear approximation and/or the neglect of coupling between the two colliding beams. Multiparticle tracking simulations also have been used, but these involve few particles, or require the fitting of a distribution function which necessarily violates the symplectic condition of the dynamics.

Ideally one would want to solve the dynamics of the beams self-consistently, that is, in such a way that: (a) the phase-space distribution function for both beams satisfies Vlasov's equation at all times, and (b) the force seen by any given particle is precisely the electromagnetic force given by Maxwell's equations for such a distribution. Although many consequences of the beam-beam interaction are understood in the various approximations, and some features of the coupled-beam problem are known to various degrees in various studies,[2] no fully satisfactory solution has yet emerged to this formidable problem.

Recently Hirata[3] has carried out several studies of the problem in another simplified model which includes some of the coupled-beam features and which incorporates the ingredient of radiation damping and noise. Thus it appears to be relevant only to e^+e^- machines. However, it invokes a particle distribution that is assumed to remain Gaussian at all times. Maxwell's equations imply a nonlinear force, and therefore an inconsistency with Vlasov's equation is automatically introduced because a Gaussian distribution cannot remain Gaussian under the action of a nonlinear force. This inconsistency is reflected in a violation of symplecticity even in the absence of radiation. Despite this shortcoming, Hirata's model has the interesting features of yielding spontaneous breaking of the symmetry between the two beams, thus apparently explaining, although only qualitatively and for unrealistic values of the parameters, the flip-flop effect and the saturation of the luminosity and beam-beam parameter at high current. However, its built-in inconsistency clouds the validity of its conclusions, and calls for further studies.

In this note we present an even simpler model, along similar lines, that has the virtue of being fully self-consistent (*i.e.*, symplectic in the absence of radiation, with Gaussian beams remaining Gaussian), since it involves the essential ingredient of a *linearized* beam-beam force (a previous note by one of us[4] was part of this effort). The consistency with Vlasov's equation is achieved at the price

of ignoring Maxwell's equations altogether, since the model assumes the force to be linear at all distances while the bunch remains finite in size. Although this is generally a good approximation for particles near the center of the bunch, it is clearly a bad one at large distance for any reasonable distribution, and the information contained in the nonlinear forces in the beam tail is lost. However, since we are interested in studying only the quadrupole modes of the coherent oscillation, the linear part of the force has the most important effect, and in this sense it is reasonable to use this approximation. Because of the consistency of our model with Vlasov's equation, our results are not tainted by violation of symplecticity, and therein lies the value of our investigation.

We need not be concerned with the detailed form of the particle distribution. All is necessary are the six (three for each bunch) 2nd order moments $\langle q^2 \rangle$, $\langle pq \rangle$ and $\langle p^2 \rangle$ of the canonical variables q, p. These are the six dynamical variables that fully describe our studies. We consider in parallel the two extreme cases of "flat beam" and "round beam" shapes, and our conclusions are qualitatively similar for both.

Our results are similar to Hirata's in some respects and different in others. As in Hirata's case, we observe the saturation of the beam-beam parameter and the luminosity as the beam intensity is increased, and the existence of stable, period–1, asymmetric solutions in which the beams are of constant but unequal size, in addition to the "normal" period–1 solutions with beams of equal size. These nontrivial solutions exist only for unrealistic values of the beam intensity. Unlike his results, however, we find, in addition, a rich structure of other solutions: there are higher-order fixed points, in which the beams are of equal size but change from turn to turn in a periodic way; and there are chaotic solutions in which the beams are of different and changing size from turn to turn with no apparent regularity, but in such a way that one beam remains preferentially bigger than the other one. In fact, a crucial difference with Hirata's case is that, in our model, it is the chaotic and higher-order fixed point solutions rather than the stable asymmetric solutions that are responsible for the saturation of the beam-beam parameter and luminosity. Furthermore, in our case, this saturation does occur at a realistic value of the beam intensity.

Our conclusions are based on a limited study; thus we present results for only one set of values of the tune and radiation parameter. A few sample calculations for other values of these parameters reveal the existence of other types of solutions, such as period–2 fixed points with unequal-size beams. Most of our results are obtained from the iteration of the six-dimensional nonlinear map for the moments of the distribution. This map has three "control parameters," namely the tune of the machine, beam intensity, and radiation parameter. It

seems a formidable problem to fully characterize this map. From the results presented here, it is reasonable to conjecture that the detailed solution is vastly more complicated.

Our results suggest a possible interpretation of observed phenomena, although the details are model-dependent. Thus, although the essence of the model may be valid, it appears that a quantitative and satisfactory explanation of the flip-flop effect and saturation of luminosity and beam-beam parameter remains an open problem.

In Section 2 we describe our model and construct the one-turn map. Section 3 describes the period–1 fixed point solutions. The simplicity of the model allows the analytic calculation of the location of the fixed point, but the stability analysis is done mostly numerically. Section 4 describes the iteration of the map and its effect on "observable" quantities. Section 5 contains the details of the results for the period–1 fixed point and iteration of the map. Section 6 contains some remarks about details and some alternatives of our model. Section 7 summarizes our conclusions.

2. Model

We consider a collider ring with only one interaction point and one bunch per beam which we may think of as the e^+ and e^- bunches, although our discussion allows for like-charged beams just as well.* We assume that the bunches collide head-on. We consider only the vertical dynamics described by the position and slope of each particle y, y', and define the normalized coordinates q, p for each beam as

$$q_\pm \equiv \frac{y_\pm}{\sqrt{\beta_y}}, \qquad p_\pm \equiv \frac{\beta_y y'_\pm + \alpha_y y_\pm}{\sqrt{\beta_y}} \tag{2.1}$$

2.1 Ingredients.

The key ingredient in our model is the beam-beam interaction which we represent by a linear kick. Under this kick the coordinates change according to

$$\begin{pmatrix} q'_\pm \\ p'_\pm \end{pmatrix} = B(k_\mp) \begin{pmatrix} q_\pm \\ p_\pm \end{pmatrix}, \qquad B(k_\mp) \equiv \begin{pmatrix} 1 & 0 \\ -k_\mp & 1 \end{pmatrix} \tag{2.2}$$

* Clearly our discussion applies equally well to a ring with K interaction regions provided the appropriate K-fold symmetry is obeyed.

where $k_\pm$ is the dimensionless strength of the linearized kick,

$$k_\pm = \frac{2\, r_0 N \beta_y}{\gamma \left\{ (\sigma_x + \sigma_y)\, \sigma_y \right\}_\pm} \equiv \frac{\beta_y}{f_\pm} \tag{2.3}$$

This is the only source of coupling between the two beams in our problem, since the strength of the kick on a particle in the e^+ beam depends on the size of the e^- beam and viceversa. In the above r_0 is the classical radius of the particle, N is the number of particles per bunch, γ is the usual relativistic factor, and $f_\pm$ is the kick's focal length. We assume N and γ to be the same for both bunches.

The $-$ sign in front of $k_\pm$ in Eq. (2.2) implies the convention that $k_\pm > 0$ for attractive kicks (opposite-charged beams) and $k_\pm < 0$ for repulsive kicks (like-charged beams).

For the flat-beam case we assume that $\sigma_{x+} = \sigma_{x-} \gg \sigma_y$ and that only σ_y is a dynamical variable. Thus we write

$$\begin{aligned} &\sigma_{x+} = \sigma_{x-} = \sqrt{\beta_x \epsilon_{x0}}, \quad \sigma_{y\pm} = \sqrt{\beta_y \left\langle q_\pm^2 \right\rangle} && \text{(flat beam)} \\ &\sigma_{x\pm} = \sigma_{y\pm} = \sqrt{\beta \left\langle q_\pm^2 \right\rangle} && \text{(round beam)} \end{aligned} \tag{2.4}$$

In the above equations ϵ_{x0} and ϵ_{y0} are nominal emittances and $\langle \cdots \rangle$ represents an average over the bunch distribution (we assume $\beta_x = \beta_y \equiv \beta$ and $\epsilon_{x0} = \epsilon_{y0} \equiv \epsilon_0$ for the round-beam case).

The essential dynamics arises from the fact that the *rms* beam sizes σ_x and σ_y are *dynamical variables.* They provide the only source of nonlinearity in the problem. Using (2.4) we express the kick strength in each case in terms of the more conventional nominal beam-beam parameter ξ_0,

$$\begin{aligned} &k_\pm = 4\pi\xi_0 \sqrt{\frac{\epsilon_{y0}}{\left\langle q_\pm^2 \right\rangle}}, \quad \xi_0 = \frac{r_0 N}{2\pi\gamma\sqrt{\epsilon_{x0}\epsilon_{y0}}} \sqrt{\frac{\beta_y}{\beta_x}} && \text{(flat beam)} \\ &k_\pm = 4\pi\xi_0 \frac{\epsilon_0}{\left\langle q_\pm^2 \right\rangle}, \quad \xi_0 = \frac{r_0 N}{4\pi\gamma\epsilon_0} && \text{(round beam)} \end{aligned} \tag{2.5}$$

This makes it clear that even though the beam-beam kick, Eq. (2.2), is linear (and therefore the dynamics symplectic), the problem of the time evolution of the moments $\langle q_\pm^2 \rangle$, $\langle p_\pm^2 \rangle$, and $\langle q_\pm p_\pm \rangle$, is nonlinear and nontrivial.

The particle also loses energy by radiation, which is restored to it by the RF cavities. We make the approximation, following Hirata, that this effect is also

represented by a localized kick, described by the stochastic transformation

$$\begin{pmatrix} q'_\pm \\ p'_\pm \end{pmatrix} = R \begin{pmatrix} q_\pm \\ p_\pm \end{pmatrix} + \hat{r}_\pm \sqrt{\epsilon_{y0}(1-\lambda^2)} \begin{pmatrix} 0 \\ 1 \end{pmatrix}, \qquad R \equiv \begin{pmatrix} 1 & 0 \\ 0 & \lambda \end{pmatrix} \tag{2.6}$$

where the $\hat{r}_\pm$ are independent random numbers distributed over the particles so that their bunch-averages over all radiation events in one turn are $\langle \hat{r}_\pm \rangle = 0$ and $\langle \hat{r}_\pm^2 \rangle = 1$. The first term in the above equation describes the momentum loss by radiation, and the second term describes the radiation noise. It is straightforward to see that the above transformation is constructed so that, in the absence of the beam-beam kick, the distribution would decay exponentially to a steady state with $\langle q^2 \rangle = \langle p^2 \rangle = \epsilon_{y0}$ and $\langle pq \rangle = 0$ (some alternatives* to (2.6) are briefly discussed in Section 6.)

The parameter λ is related to the "damping decrement" δ by $\lambda = \exp(-2\delta)$, and $\delta = T_0/T_d$ where T_0 is the revolution period and T_d is the damping time, *i.e.*, the time it takes for $\langle pq \rangle$ to reach $1/e$ of its initial value due to radiation. In practice, for existent e^+e^- machines, δ is a very small number, of order $10^{-3} - 10^{-4}$, so $\lambda \lesssim 1$. For our applications, however, we will let λ be any number in the range $(0,1)$. Likewise, the beam-beam parameter ξ_0 has typical values of order $10^{-2} - 10^{-4}$ but, for our purposes, we will allow it to have any value.

The third and final ingredient for our model is a linear transport through a phase advance $2\pi\nu$. In this case the transformation is

$$\begin{pmatrix} q'_\pm \\ p'_\pm \end{pmatrix} = T \begin{pmatrix} q_\pm \\ p_\pm \end{pmatrix}, \qquad T \equiv \begin{pmatrix} \cos(2\pi\nu) & \sin(2\pi\nu) \\ -\sin(2\pi\nu) & \cos(2\pi\nu) \end{pmatrix} \tag{2.7}$$

2.2 One-turn map.

We complete our model by combining the above ingredients into a map. We assume that the bunches collide, then are transported through the entire length of the ring, then radiate, then collide again, etc. (see Section 6 below for comments regarding another order). Schematically, they experience the transformations $B \to T \to R \to B \to \cdots$ Therefore, if we construct a surface of section just before

* We are grateful to Bob Siemann for remarks concerning this point.

the beam-beam kick, the map that relates turn $n+1$ to turn n is represented by

$$\begin{pmatrix} q_\pm \\ p_\pm \end{pmatrix}_{n+1} = M(k_{\mp,n}) \begin{pmatrix} q_\pm \\ p_\pm \end{pmatrix}_n + \hat{r}_\pm \sqrt{\epsilon_{y0}(1-\lambda^2)} \begin{pmatrix} 0 \\ 1 \end{pmatrix} \tag{2.8}$$

where the map matrix M is given by

$$M(k_\mp) \equiv RTB(k_\mp) = \begin{pmatrix} C - k_\mp S & S \\ -\lambda(S + k_\mp C) & \lambda C \end{pmatrix} \tag{2.9}$$

in which $C = \cos(2\pi\nu)$, $S = \sin(2\pi\nu)$, and ν is the tune of the machine (for a K-fold symmetric ring ν is the phase advance/2π and λ the radiation parameter of one symmetry sector, respectively).

A six-dimensional deterministic map is obtained from the above by taking the averages of the bilinear combinations of q and p over their corresponding particle distribution, and averaging these over the radiation events for one turn. Thus

$$\begin{bmatrix} \langle q_+^2 \rangle \\ \langle p_+ q_+ \rangle \\ \langle p_+^2 \rangle \\ \langle q_-^2 \rangle \\ \langle p_- q_- \rangle \\ \langle p_-^2 \rangle \end{bmatrix}_{n+1} = \begin{bmatrix} \widetilde{M}(k_{-,n}) & 0 \\ 0 & \widetilde{M}(k_{+,n}) \end{bmatrix} \begin{bmatrix} \langle q_+^2 \rangle \\ \langle p_+ q_+ \rangle \\ \langle p_+^2 \rangle \\ \langle q_-^2 \rangle \\ \langle p_- q_- \rangle \\ \langle p_-^2 \rangle \end{bmatrix}_n + \epsilon_{y0}(1-\lambda^2) \begin{bmatrix} 0 \\ 0 \\ 1 \\ 0 \\ 0 \\ 1 \end{bmatrix} \tag{2.10}$$

where the 3×3 matrix $\widetilde{M}$ is obtained from M by

$$\widetilde{M} = \begin{pmatrix} M_{11}^2 & 2M_{11}M_{12} & M_{12}^2 \\ M_{11}M_{21} & M_{11}M_{22} + M_{12}M_{21} & M_{12}M_{22} \\ M_{21}^2 & 2M_{21}M_{22} & M_{22}^2 \end{pmatrix} \tag{2.11}$$

It is easy to verify that M and $\widetilde{M}$ have unit determinant if and only if $\lambda = 1$ (*i.e.*, no radiation), as it should be the case.

Note that the six-dimensional map (2.10) is nonlinear because $\widetilde{M}(k_\pm)$ depends on $\langle q_\pm^2 \rangle_n$ *via* $k_{\pm,n}$. When written in terms of $k_\pm$ the map has the same form for both flat and round beams; the difference comes only in the definition of $k_\pm$, Eq. (2.5).

The map can be studied in the conventional way by starting with a specified set of values for all six moments and iterating. We will provide the results in a later section. However, because of the relative simplicity of the map, it is possible and worthwhile to look for the simplest possible solutions, namely period–1 fixed points, which can be done analytically, and study their stability by analyzing the stability matrix.

3. Period–One Fixed Points

3.1 Location of the fixed points.

The defining condition for a period–1 fixed point is $\langle\cdots\rangle_{n+1} = \langle\cdots\rangle_n$ for all six moments. Thus we obtain

$$\begin{bmatrix} \langle q_+^2\rangle \\ \langle p_+q_+\rangle \\ \langle p_+^2\rangle \\ \langle q_-^2\rangle \\ \langle p_-q_-\rangle \\ \langle p_-^2\rangle \end{bmatrix} = \epsilon_{y0}(1-\lambda^2) \begin{bmatrix} 1-\widetilde{M}(k_-) & 0 \\ 0 & 1-\widetilde{M}(k_+) \end{bmatrix}^{-1} \begin{bmatrix} 0 \\ 0 \\ 1 \\ 0 \\ 0 \\ 1 \end{bmatrix} \tag{3.1}$$

This represents a set of six coupled nonlinear equations for six unknowns. However, because the matrix is block-diagonal, we need to invert only a 3×3 matrix. Furthermore, since $\widetilde{M}$ does not depend on $\langle pq\rangle$ nor $\langle p^2\rangle$, the set consists of two equations for two unknowns, namely $\langle q_+^2\rangle$ and $\langle q_-^2\rangle$. These correspond to rows 1 and 4 of the above matrix equation.

The inverse of the 3×3 matrix is very simple. We obtain

$$\begin{bmatrix} \\ 1-\widetilde{M}(k) \\ \\ \end{bmatrix}^{-1} \begin{bmatrix} 0 \\ 0 \\ 1 \end{bmatrix} = \frac{S^2}{D(k)} \begin{bmatrix} \lambda+1 \\ k\lambda \\ \lambda+1+2k\cot(2\pi\nu)-k^2(1-\lambda) \end{bmatrix} \tag{3.2}$$

where k is either k_+ or k_-, and

$$\begin{aligned} D(k) &\equiv \det\left(1-\widetilde{M}(k)\right) \\ &= (1-\lambda^2)(\lambda+1)S^2\left[1+\frac{2k}{\lambda+1}\cot(2\pi\nu)-\frac{k^2}{(\lambda+1)^2}\right] \end{aligned} \tag{3.3}$$

Note that, although the determinant vanishes in the limit $\lambda\to 1$ (no-radiation limit), the equations are regular on account of the $(1-\lambda^2)$ factor in Eq. (3.1).

Thus a perfectly regular solution for the period-1 fixed point exists for $\lambda = 1$, which is given explicitly in Section 6. However, the stability analysis shows in this case that the equilibrium is either marginal or unstable because the eigenvalues are such that either they all lie on the unit circle, or there is at least one greater than unity in absolute value.

So far the discussion applies equally well to flat beams as it does to round beams. In order to proceed we must now specialize the equations to either case by expressing $\langle q_+^2 \rangle$ and $\langle q_-^2 \rangle$ in terms of k_+ and k_-. Eq. (3.3) suggests using the scaled variables x and y defined by

$$k_+ \equiv (\lambda + 1)x, \qquad k_- \equiv (\lambda + 1)y \tag{3.4}$$

in terms of which Eq. (2.5) reads

$$\begin{aligned} x &= \frac{4\pi\xi_0}{\lambda+1}\sqrt{\frac{\epsilon_{y0}}{\langle q_+^2 \rangle}}, \qquad y = \frac{4\pi\xi_0}{\lambda+1}\sqrt{\frac{\epsilon_{y0}}{\langle q_-^2 \rangle}} \qquad \text{(flat beam)} \\ x &= \frac{4\pi\xi_0}{\lambda+1}\frac{\epsilon_0}{\langle q_+^2 \rangle}, \qquad y = \frac{4\pi\xi_0}{\lambda+1}\frac{\epsilon_0}{\langle q_-^2 \rangle} \qquad \text{(round beam)} \end{aligned} \tag{3.5}$$

Thus the period-1 fixed point equations for the flat-beam case are

$$\begin{aligned} x^2 &= \rho^2(1 + 2\chi y - y^2) \\ y^2 &= \rho^2(1 + 2\chi x - x^2) \qquad \text{(flat beam)} \end{aligned} \tag{3.6}$$

and for the round-beam case,

$$\begin{aligned} x &= \rho\,(1 + 2\chi y - y^2) \\ y &= \rho\,(1 + 2\chi x - x^2) \qquad \text{(round beam)} \end{aligned} \tag{3.7}$$

where we have defined

$$\rho \equiv \frac{4\pi\xi_0}{\lambda+1}, \qquad \chi \equiv \cot(2\pi\nu) \tag{3.8}$$

for both cases. Note, however, that the definition of ξ_0 in terms of the machine and beam parameters is different for both cases, as per Eq. (2.5).

Once x and y have been found, the location of the fixed point is completed by finding $\langle pq \rangle$ and $\langle p^2 \rangle$. These are obtained from Eq. (3.2), which yields the

following relations, valid only at the fixed point:

$$\begin{aligned} \frac{\langle p_+ q_+ \rangle}{\langle q_+^2 \rangle} &= \lambda y \\ \frac{\langle p_+^2 \rangle}{\langle q_+^2 \rangle} &= 1 + 2\chi y - (1-\lambda^2) y^2 \end{aligned} \tag{3.9}$$

with corresponding relations for the e^- beam, found by exchanging $x \leftrightarrow y$.

Eqs. (3.6) and (3.7) represent the intersection of two ellipses and two parabolas, respectively, in the $x-y$ plane. They are mirror images of each other about the main diagonal. Depending on the values of ρ and χ there can be 4, 2, or no real solutions. Even if a solution is real it is not necessarily physical because the sign is important: the solutions for x and y must have the same sign (opposite-sign solutions violate Newton's 2nd law). If we adopt the convention that ξ_0 (and therefore ρ) is always positive, then the $+$ solutions are physical for the opposite-charge case, while the $-$ solutions are physical for the like-charge case (equivalently, one may choose ξ_0 to be > 0 for the opposite-charge case and < 0 for the like-charge case, and seek only positive solutions for x and y).

Eqs. (3.6–7) admit $x = y$ and $x \neq y$ solutions, corresponding to equal-size beams and unequal-size beams (the stability of each is discussed later).

Equal-size beam solutions. The equal-size beam solutions are obtained by setting $x = y$ in Eqs. (3.6–7), which yield

$$x_\pm = \frac{\rho}{1+\rho^2}\left[\chi\rho \pm \sqrt{(\chi\rho)^2 + 1 + \rho^2}\right], \qquad \text{(flat beam)} \tag{3.10}$$

and

$$x_\pm = \frac{1}{2\rho}\left[2\chi\rho - 1 \pm \sqrt{(2\chi\rho - 1)^2 + 4\rho^2}\right], \qquad \text{(round beam)} \tag{3.11}$$

Note that they are always real, and that $x_+ > 0$, $x_- < 0$ for all values of χ and ρ. In the weak-beam limit, $\rho \to 0$, the opposite-charge solutions x_+ for either flat or round beam are

$$\begin{aligned} \langle q^2 \rangle &= \epsilon_{y0}\,(1 - 2\chi\rho + \cdots) \\ \langle pq \rangle &= \epsilon_{y0}\,(\lambda\rho + \cdots) \\ \langle p^2 \rangle &= \epsilon_{y0}\,(1 + \cdots) \end{aligned} \tag{3.12}$$

where $\cdots$ represents terms of order ρ^2 or higher. Note the correct limit in the absence of beam-beam kick.

Unequal-size beam solutions. The unequal-size beams solutions are most easily found by subtracting the two equations in (3.6) and (3.7) and dividing through by $x - y$, which yields

$$\begin{aligned} x + y &= -\frac{2\chi\rho^2}{1-\rho^2}, && \text{(flat beam)} \\ x + y &= \frac{2\chi\rho + 1}{\rho}, && \text{(round beam)} \end{aligned} \tag{3.13}$$

and then solving for x and y. One then finds, for flat beam,

$$\begin{Bmatrix} x \\ y \end{Bmatrix} = -\frac{\chi\rho^2}{1-\rho^2} \pm \frac{1}{1-\rho^4}\sqrt{\rho^2(1+\rho^2)\left[(1-\rho^2)^2 - (3-\rho^2)(\chi\rho)^2\right]} \tag{3.14}$$

and, for round beam,

$$\begin{Bmatrix} x \\ y \end{Bmatrix} = \frac{1}{2\rho}\left[2\chi\rho + 1 \pm \sqrt{(2\chi\rho - 1)^2 - 4(1-\rho^2)}\right] \tag{3.15}$$

The solutions are real only for certain values of χ and ρ. The reality conditions are

$$\begin{aligned} (3-\rho^2)(\chi\rho)^2 &< (1-\rho^2)^2 && \text{(flat beam)} \\ (2\chi\rho - 1)^2 &> 4(1-\rho^2) && \text{(round beam)} \end{aligned} \tag{3.16}$$

which are obviously satisfied for $\rho > \sqrt{3}$ and $\rho > 1$, respectively, but are nontrivial for smaller values of ρ.

In addition to being real, the solutions for x and y must have the same sign in order to make physical sense. The conditions on χ and ρ are most easily found by setting the product xy to be positive. Thus we find

$$\begin{aligned} (2\chi\rho)^2 &> (1-\rho^2)^2 && \text{(flat beam)} \\ 2\chi\rho &> \rho^2 - 1 && \text{(round beam)} \end{aligned} \tag{3.17}$$

By combining constraints (3.16) and (3.17) we find the regions in the $\chi - \rho$ (or $\nu - \rho$) plane in which these unequal-size solutions are physical. They are shown as the shaded areas in Figs. 1 and 2.

3.2 Stability of the period–1 fixed points.

In order to study the stability of the fixed point we expand the map (2.10) infinitesimally close to it, which is possible because the map is analytic there. In this approximation the map is linear and homogeneous, and the standard eigenvalue analysis can be used.

If we define the three-component, dimensionless vectors

$$\mathbf{X}_n = \frac{1}{\epsilon_{y0}} \begin{bmatrix} \langle q_+^2 \rangle \\ \langle p_+ q_+ \rangle \\ \langle p_+^2 \rangle \end{bmatrix}_n \qquad \mathbf{Y}_n = \frac{1}{\epsilon_{y0}} \begin{bmatrix} \langle q_-^2 \rangle \\ \langle p_- q_- \rangle \\ \langle p_-^2 \rangle \end{bmatrix}_n \tag{3.18}$$

then the map (2.10) reads

$$\begin{bmatrix} \mathbf{X} \\ \mathbf{Y} \end{bmatrix}_{n+1} = \begin{bmatrix} \widetilde{M}(y_n) & 0 \\ 0 & \widetilde{M}(x_n) \end{bmatrix} \begin{bmatrix} \mathbf{X} \\ \mathbf{Y} \end{bmatrix}_n + (1-\lambda^2) \begin{bmatrix} \mathbf{e} \\ \mathbf{e} \end{bmatrix} \tag{3.19}$$

where $\mathbf{e} = \mathrm{col}(0,0,1)$ (we have made explicit the fact that $\widetilde{M}(\mathbf{X})$ depends only on the first component X_1, which we have traded off for x according to Eqs. (3.4–5)).

We denote the fixed point as $\mathbf{X}$, $\mathbf{Y}$ and write $\mathbf{X}_n = \mathbf{X} + \Delta\mathbf{X}$, $\mathbf{X}_{n+1} = \mathbf{X} + \Delta\mathbf{X}'$, and similarly for $\mathbf{Y}_n$. We expand the map to lowest order and obtain the stability matrix Σ,

$$\begin{bmatrix} \Delta\mathbf{X}' \\ \Delta\mathbf{Y}' \end{bmatrix} = \Sigma(x,y) \begin{bmatrix} \Delta\mathbf{X} \\ \Delta\mathbf{Y} \end{bmatrix} \tag{3.20}$$

which has the form

$$\Sigma(x,y) = \begin{bmatrix} \widetilde{M}(y) & N(x,y) \\ N(y,x) & \widetilde{M}(x) \end{bmatrix} \tag{3.21}$$

and where

$$N(x,y) = \begin{bmatrix} & 0 & 0 \\ \mathbf{V}(x,y) & 0 & 0 \\ & 0 & 0 \end{bmatrix} \tag{3.22}$$

$$\mathbf{V}(x,y) = \frac{\partial \widetilde{M}(Y_1)}{\partial Y_1} \mathbf{X}$$

The expressions for $\mathbf{X}$ and $\partial\widetilde{M}(y)/\partial y$ are, for either flat or round beam,

$$\mathbf{X} = \frac{1}{1+2\chi y - y^2}\begin{bmatrix} 1 \\ \lambda y \\ 1+2\chi y-(1-\lambda^2)y^2 \end{bmatrix}$$

$$\frac{\partial\widetilde{M}(y)}{\partial y} = (\lambda+1)\begin{bmatrix} 2S((\lambda+1)Sy-C) & -2S^2 & 0 \\ \lambda(2(\lambda+1)SCy+S^2-C^2) & -2\lambda SC & 0 \\ 2\lambda^2C((\lambda+1)Cy+S) & -2\lambda^2C^2 & 0 \end{bmatrix} \tag{3.23}$$

So far the equations are the same for both flat-beam and round-beam cases. To proceed, we note from Eq. (3.5) that

$$\begin{aligned} X_1 &= \rho^2/x^2, \qquad Y_1 = \rho^2/y^2 \qquad \text{(flat beam)} \\ X_1 &= \rho/x, \qquad Y_1 = \rho/y \qquad \text{(round beam)} \end{aligned} \tag{3.24}$$

which are needed to relate $\partial/\partial y$ to $\partial/\partial Y_1$. Combining the above equations together with the fixed-point conditions (3.6–7), we obtain

$$\mathbf{V}(x,y) = -(\lambda+1)\ J(x,y)\begin{bmatrix} S(Sy-C) \\ \lambda(2SCy-C^2+S^2)/2 \\ \lambda^2C(Cy+S) \end{bmatrix} \tag{3.25}$$

where $J(x,y)$ is

$$\begin{aligned} J(x,y) &= y^3/x^2 \qquad \text{(flat beam)} \\ J(x,y) &= 2y^2/x \qquad \text{(round beam)} \end{aligned} \tag{3.26}$$

This completes the definition of the stability matrix. The analysis proceeds in the conventional way: for given values of χ, ρ and λ we find x and y from Eqs. (3.10–11) or (3.14–15), construct the stability matrix and find its eigenvalues. If all six eigenvalues are less than unity in absolute value we call the solution stable; otherwise it is unstable. One property of the stability matrix, which is useful to check the numerical calculations, is that the determinant has the value

$$\det\Sigma(x,y) = \lambda^6 \tag{3.27}$$

for both the $x = y$ and $x \neq y$ cases, regardless of whether the beam is flat or round. This implies that, if the motion is stable, the eigenvalues are of order λ in absolute value.

Sample results for the size and stability of oppositely-charged beams are shown in Figs. 3 and 4, for flat and round beams, respectively. They are discussed in detail in Section 5.

4. Iteration of the Map

By starting with a given set of values for $\mathbf{X}$ and $\mathbf{Y}$ we iterate the map (3.19) and see whether it converges to fixed point, or behaves chaotically, or diverges. We provide only a sample case in Figs. 5 and 6 for flat and round beams respectively, for oppositely-charged beams. The details are discussed in the following section.

The physical effects of the iteration of the map can be seen by looking at "observable" quantities such as the luminosity, or the effective beam-beam parameter. They are given by

$$\begin{aligned} \mathcal{L} &= \frac{N^2 f}{8\pi\sqrt{\beta_x\beta_y\epsilon_x\epsilon_y}}, \qquad \xi = \frac{r_0 N}{2\pi\gamma\sqrt{\epsilon_x\epsilon_y}}\sqrt{\frac{\beta_y}{\beta_x}} \qquad \text{(flat beam)} \\ \mathcal{L} &= \frac{N^2 f}{4\pi\beta\epsilon}, \qquad \xi = \frac{r_0 N}{4\pi\gamma\epsilon} \qquad \text{(round beam)} \end{aligned} \tag{4.1}$$

where f is the bunch collision frequency, N the number of particles per bunch, and ϵ_x, ϵ_y, ϵ are the actual values of the emittances (for flat beam, $\epsilon_x = \epsilon_{x0}$). The "nominal" values $\mathcal{L}_0$ and ξ_0 are the same as the above, except for the replacements $\epsilon_x, \epsilon_y \to \epsilon_{x0}, \epsilon_{y0}$. Now in our model ϵ_y and ϵ are given by

$$\begin{aligned} \epsilon_y &= \left(\langle q_+^2\rangle + \langle q_-^2\rangle\right)/2 \qquad \text{(flat beam)} \\ \epsilon &= \left(\langle q_+^2\rangle + \langle q_-^2\rangle\right)/2 \qquad \text{(round beam)} \end{aligned} \tag{4.2}$$

Thus a quantity that measures the physical effects of our model is the "enhancement factor" E defined by $E \equiv \mathcal{L}/\mathcal{L}_0 = \xi/\xi_0$,

$$\begin{aligned} E &= \sqrt{\frac{\epsilon_{y0}}{\epsilon_y}} = \sqrt{\frac{2}{X_1+Y_1}} = \frac{xy}{\rho}\sqrt{\frac{2}{x^2+y^2}} \qquad \text{(flat beam)} \\ E &= \frac{\epsilon_0}{\epsilon} = \frac{2}{X_1+Y_1} = \frac{2\,xy}{\rho(x+y)} \qquad \text{(round beam)} \end{aligned} \tag{4.3}$$

In the weak-beam limit, $\rho \to 0$, only the equal-size solutions are stable. For the opposite-charge case E behaves linearly with ρ,

$$\begin{aligned} E &= 1 + \chi\rho + \cdots \qquad \text{(flat beam)} \\ E &= 1 + 2\chi\rho + \cdots \qquad \text{(round beam)} \end{aligned} \tag{4.4}$$

and all quantities take on their nominal values at $\rho = 0$, which gives them a precise meaning in our context. We plot E *vs.* ρ in Figs. 7 and 8.

5. Results

The results for the location of the period–1 fixed point show that: (a) "normal" solutions (*i.e.*, beams of constant and equal size) exist for flat and round beam shape for all values of ν and ρ, and do not depend separately on λ; (b) for the flat-beam case, constant solutions with beams of unequal size exist only in certain regions of the $\nu - \rho$ plane both for like-charged and opposite-charged beams, as shown in Fig. 1; and (c) for the round-beam case, constant solutions with beams of unequal size exist only in a certain region of the $\nu - \rho$ plane for opposite-charged beams, as shown in Fig. 2, and not at all for like-charged beams.

All results presented below for the stability of the period–1 fixed point and for the iteration of the map are for oppositely-charged beams and for $\nu = 0.15$ and $\delta = 0.07$ ($\lambda = 0.8694$), both for flat- and round-beam cases. Although this is an unrealistically large value of δ, which corresponds to a synchrotron radiation energy loss of $\sim 13\%$ per turn, we hasten to emphasize that *all our results are quantitatively similar* for any λ close enough to 1. This is because our model is symplectic in the absence of radiation and therefore all our results have a smooth $\lambda \to 1$ limit. This is shown explicitly for the period–1 fixed point solutions in the section below. Of course the case $\lambda = 1$ is different from λ infinitesimally below 1 because, for example, the motion would not be considered stable if all the eigenvalues of the stability matrix were unity in absolute value, whereas it would be considered stable if the eigenvalues were infinitesimally less than 1 in absolute value. The practical advantage of choosing a fairly large δ, as we do here, is that the convergence of the map iteration is relatively fast.

Results for the beam size and stability of the period–1 fixed point are shown in Figs. 3 and 4, for flat and round beams, respectively, in which we plot the normalized *rms* beam sizes $\sqrt{X_1}$ and $\sqrt{Y_1}$ *vs.* ρ. Equal-size beam solutions exist for all values of ρ; unequal-size beam solutions exist only in a finite range of values of ρ, represented by the two branches of the curve. The solid portions of the lines indicate stability, the dotted portions instability.

If the period–1 solution is unstable it means that the motion may have higher-order stable fixed points, or chaotic behavior, or it may be truly unstable. Even if the solutions are stable, they may coexist with other stable higher-order fixed points. This is illustrated by iterating the map (3.19), which we show in Figs. 5 and 6 for flat and round beams respectively. By starting with a given set of values for $\mathbf{X}$ and $\mathbf{Y}$ we iterate the map and see whether it converges to a fixed point, or behaves chaotically, or diverges. The nature of the solution depends not only on the parameters χ, ρ, λ, but also on the starting point $\mathbf{X}_0$, $\mathbf{Y}_0$. It is almost

impossible to give a full description of the map in this six-dimensional space, so we provide only sample "runs." The dots represent chaotic behavior, in which the two beams change in size from turn to turn with no apparent regularity, but in such a way that one of them remains preferentially larger. The symbol + represents period–1 fixed points in which the beams are of equal or unequal size, depending on the value of ρ (they correspond to the beam sizes shown in Figs. 3 and 4). The symbols $\times$, $\diamond$ and $\square$ represent period–2, –3, and –4 fixed points with beams of equal size. These solutions start to appear at $\rho \simeq 0.41$ for flat beams and $\rho \simeq 0.27$ for round beams. A bifurcation with the period doubling from 2 to 4 occurs near $\rho = 1.7$ for the round-beam case. There are apparently no chaotic solutions with beams of equal size, nor fixed points of period higher than 1 with beams of unequal size. We have not found other types of solutions than the ones described because of the limited accuracy of our search, but of course they may well exist (a spot check for $\nu = 0.176$ did reveal a period–2 solution with unequal-size beams).

Whenever there is more than one possible solution, the one to which the map converges for given ρ, χ depends on the initial conditions $\mathbf{X}_0, \mathbf{Y}_0$. For $\rho \simeq 0.5$ for the flat-beam case, and $\rho \simeq 0.3$ for the round-beam case, the chaotic solutions are the most stable. Besides limited ranges of ρ around these values, generally speaking, the period–1 fixed point is the most stable unless period–2 or period–3 fixed points coexist with it. In this case the period–2 fixed point is the most stable for the flat-beam case, while the period–3 fixed point is the most stable for the round-beam case. By "most stable" we mean that the size of the region of values of $\mathbf{X}_0, \mathbf{Y}_0$ which converge to these solutions seems to be largest, so therefore this is the most likely solution to be reached by the map. For this reason we use only these to evaluate the enhancement factor E (we compute its average over the period of the fixed point). Figs. 7 and 8 show E *vs.* ρ for flat and round beams respectively. Note that E increases to a maximum and then decreases roughly like $1/\rho$. Since $\rho \propto N$, this means that the luminosity increases only linearly with beam current, and the beam-beam parameter saturates beyond this point.

6. Remarks

6.1 Order of the kicks in the map definition.

Refs. 3 and 4 use the order $B \to R \to T$ in the definition of the map rather than $B \to T \to R$ as we do here. Since the two become identical for $\lambda = 1$ and since our $\lambda \to 1$ limit is smooth, the difference is not significant for realistic values of λ. For the period–1 fixed point, it turns out, the only difference that the other order implies is a different definition for ρ, which is $\rho = 4\pi\xi_0\lambda/(\lambda+1)$ instead of (3.8).

6.2 $\lambda = 1$ limit of the period–1 fixed point.

Since our model is symplectic in the absence of radiation, the limit $\lambda \to 1$ is perfectly smooth. The beam size of the period–1 fixed point solutions does not depend on λ explicitly, so it is still given by Eqs. (3.10–11) and (3.14–15). The stability analysis, however, is simpler. In the case of unequal-size beam solutions, $x \neq y$, the characteristic polynomial $P(\mu) \equiv \det[\Sigma(x,y) - \mu \mathrm{I}]$ factorizes in the form

$$P(\mu) = (\mu - 1)^2(\mu^4 + \cdots + 1) \tag{6.1}$$

and, in the case of equal-size solutions, $x = y$, it factorizes even more,

$$P(\mu) = (\mu - 1)^2(\mu^2 - 2a\mu + 1)(\mu^2 - 2b\mu + 1) \tag{6.2}$$

where

$$a = (Sx - C)(Sx - 2C) - 1, \qquad b = (3Sx - 2C)(Sx - C) - 1 \tag{6.3}$$

for flat beam, and

$$a = -2C(Sx - C) - 1, \qquad b = 2(Sx - C)(2Sx - C) - 1 \tag{6.4}$$

for round beam. Therefore, in this case of $x = y$ and $\lambda = 1$ the eigenvalues are

$$\mu_n = \begin{cases} 1,\ 1 \\ a \pm i\sqrt{1 - a^2} \\ b \pm i\sqrt{1 - b^2} \end{cases} \tag{6.5}$$

which lie on the unit circle if $-1 < a < 1$ and $-1 < b < 1$, in which case the stability is "marginal," or are real otherwise, in which case there is instability. Depending on the values of ν and ρ, both possibilities can be realized.

6.3 Alternatives to the radiation kick.

It is possible to describe the radiation effects in a more realistic way than by a single kick and so that the equilibrium distribution satisfies $\langle q^2 \rangle = \langle p^2 \rangle = \epsilon_{y0}$ and $\langle pq \rangle = 0$ in the absence of beam-beam kick. For example, one can imagine that there are K radiation kicks around the ring, each one described by an equation similar to (2.6) but with λ replaced by $\lambda^{1/K}$ and with a different $\hat{r}_{\pm}$, and that the ring is divided up into K arc segments, one between every two radiation kicks, and each with a phase advance $2\pi\nu/K$. By taking the limit $K \to \infty$ one then finds the transformation for the combined transport and radiation between beam-beam kicks. We have done this calculation algebraically, and the resultant map is fairly complicated. The equation for the beam size of the period–1 fixed point cannot be solved analytically, although it would be a simple matter to use this map in the tracking of the moments. A very simplified (but less realistic) special case of the above is found when ν is an integer and there are radiation kicks like (2.6) every 1/4–integer. The resultant effective kick is like (2.6) except that $\lambda \to \sqrt{\lambda}$ and that both q and p are kicked. The resultant equation for the period–1 fixed point is quite complicated. An even simpler description is to assume that the kick is in q rather than p; in this case the equation for the beam size of the period–1 fixed point is a cubic for flat beams but it is still a quadratic for round beams. A few spot checks for the period–1 fixed point and the other solutions showed that they are quantitatively different from those presented here, although the general qualitative features of the results are similar.

It has been recently pointed out[5] that if one does represent the radiation effects by one single kick, as we have done here, this kick must be located at a symmetry point of the lattice ($\beta' = 0$) and it must be such that the strength of the noise term is scaled so that it corresponds to the beam-beam–perturbed β–function. Otherwise there is a mismatch with the phase ellipse which leads to spurious emittance growth. This conclusion has been reached by multiparticle tracking simulations in which the two beams are forced to remain equal in size. In our problem the radiation kick is located immediately before the beam-beam kick, and the strength of the noise term is scaled with the "bare" β–function; however we do not see evidence of this emittance growth. Indeed, the equal-size period–1 solutions have a fairly constant size for a large range of ρ. This apparent contradiction is under investigation.

7. Conclusions

We have constructed a dynamical model of the beam-beam interaction that is consistent with Vlasov's equation, whose key ingredient is a linearized beam-beam force. The model has features such as saturation of the luminosity and beam-beam parameter as a function of current, and asymmetric solutions in which otherwise identical bunches reach an equilibrium state with different sizes. The model also has other solutions, in which the beam sizes change chaotically with time, and also fixed point solutions with period higher than one. Because the model is symplectic in the absence of radiation, all our results are quantitatively similar for any value of λ sufficiently close to 1.

There exist period–1 solutions with beams of unequal size, which are necessary to explain the flip-flop phenomenon, that are real for all values of ρ; however, these solutions are not always stable and, furthermore, are unnatural for small ρ. By this we mean that they require a very delicate relationship between ν and ρ, as can be seen from Figs. 1 and 2. Therefore these solutions, although suggestive, are probably not realistic candidates for an explanation of the flip-flop phenomenon.

For realistic values of the beam intensity, *i.e.*, $\rho \lesssim 0.5$, only three types of solutions exist, are stable and natural: "normal" solutions with beams of equal and constant size, chaotic solutions in which the beams change randomly from turn to turn with one of them remaining preferentially bigger than the other one, and higher-order fixed point solutions with equal-size beams. The saturation of the luminosity and beam-beam parameter occur at a nominal beam-beam parameter $\xi_0 \simeq \rho/2\pi \simeq 0.065$ for flat beam and $\simeq 0.043$ for round beam. Thus in our model this saturation mechanism is due to the appearence of a chaotic region followed by a higher-order fixed point rather than a bifurcation. This seems to be a key difference with Hirata's result.[3]

The stability analysis of the period–1 fixed point shows large regions of instability, as seen in Figs. 3 and 4. For these regions the iteration of the map reveals a rich structure of chaotic behavior and higher–order fixed points, shown in Figs. 5 and 6. Apparently this structure is due to the linear nature of the force, since it is absent for the case in which the force vanishes at large distance.[3]

It may be possible to extend our model to describe realistic beam distributions consistently with Maxwell's equations, in addition to Vlasov's equation, by considering all higher-order moments of the distribution function. Such a method would involve an infinite set of coupled nonlinear equations, but a systematic approximation may be one in which it is truncated at higher and higher orders.

Our model shows a new possible mechanism for the explanation of the saturation of the luminosity and beam-beam parameter, namely the appearence of a chaotic solution followed by a higher-order fixed point. This saturation occurs, in our model, at realistic values of the beam intensity. However, the problem of a quantitative and self-consistent explanation of the flip-flop phenomenon remains open.

ACKNOWLEDGEMENTS

We are grateful to Kohji Hirata and Bob Siemann for discussions.

REFERENCES

1. M. Month and J. C. Herrera, *eds.*, "Nonlinear Dynamics and the Beam-Beam Interaction, (BNL, 1979)," AIP Conference Proceeding No. 57.
2. C. Pellegrini and A. M. Sessler, Proc. VI Intl. Conf. on High Energy Accelerators, Cambridge, 1967, p.135; A. Piwinski, "Coherent Beam Breakup due to Space-Charge," Proc. VIII Intl. Conference on High Energy Accelerators, CERN, 1971, p.357; F. Amman, "Longitudinal Instability due to Beam-Beam Interaction in Electron Storage Rings," LNF 71/82, 1971; Ya. S. Derbenev, "Collective Instability of Compensated Colliding Beams," proceedings of the III All Union Part. Accel. Conf., Moscow (1973) p. 382; N. N. Chau and D. Potaux, "Stabilité des Oscillations Transverses Dans un Anneau à Charge d'Espace Compensée," Orsay Technical Report 5-74 (1974) and 2-75 (1975); A. W. Chao and E. Keil, "Coherent Beam-Beam Effect," SLAC/PEP-300 (1979); E. Keil, "Theoretical Aspects of the Beam-Beam Interaction," Proc. XI Intl. Conf. on High Energy Accelerators, CERN, 1980, p.759; R. E. Meller and R. H. Siemann, "Coherent Normal Modes of Colliding Beams," IEEE Trans. Nucl. Sci. **NS-28**, 2431 (1981); Y. Kamiya and A. W. Chao, "Stability of the Coherent Quadrupole Oscillations by the Beam-Beam Interaction," SLAC/AP-8, October 1983, and "Coherent Synchro-Betatron Oscillations Excited by the Beam-Beam Interaction," SLAC/AP-10, 1983; J. D. Bjorken, "Coupled Bunch Instabilities in a $\bar{p}p$ Collider," Workshop on $\bar{p}p$ Options for the Supercollider, Univ. of Chicago, 1984, Fermilab-Conf-84/29-THY (1984); A. W. Chao and R. D. Ruth, "Coherent Beam-Beam Instability in Colliding Beam Storage Rings," Part. Accel. **16**, 201 (1985).

3. K. Hirata, "Solvable Model of the Beam-Beam Limit in e^+e^- Colliding Rings," *Phys. Rev. Lett.* **58**, 25 (1987) (*erratum:* **58**, 1798 (1987)); "Solvable Model, Flip-Flop Hysteresis and Catastrophe in e^+e^- Colliding Storage Rings," KEK Preprint 86-102, February 1987; "Solvable Model of the Beam-Beam Effects in e^+e^- Colliding Storage Rings," KEK Preprint 87-76, September 1987.
4. K.-Y. Ng, "Linear Beam-Beam Effects for Round Beams," SSC-161, January 1988.
5. R. Siemann and S. Krishnagopal, Cornell University CESR notes CBN 88–1, May 1988 and CBN 88–2, June 1988.

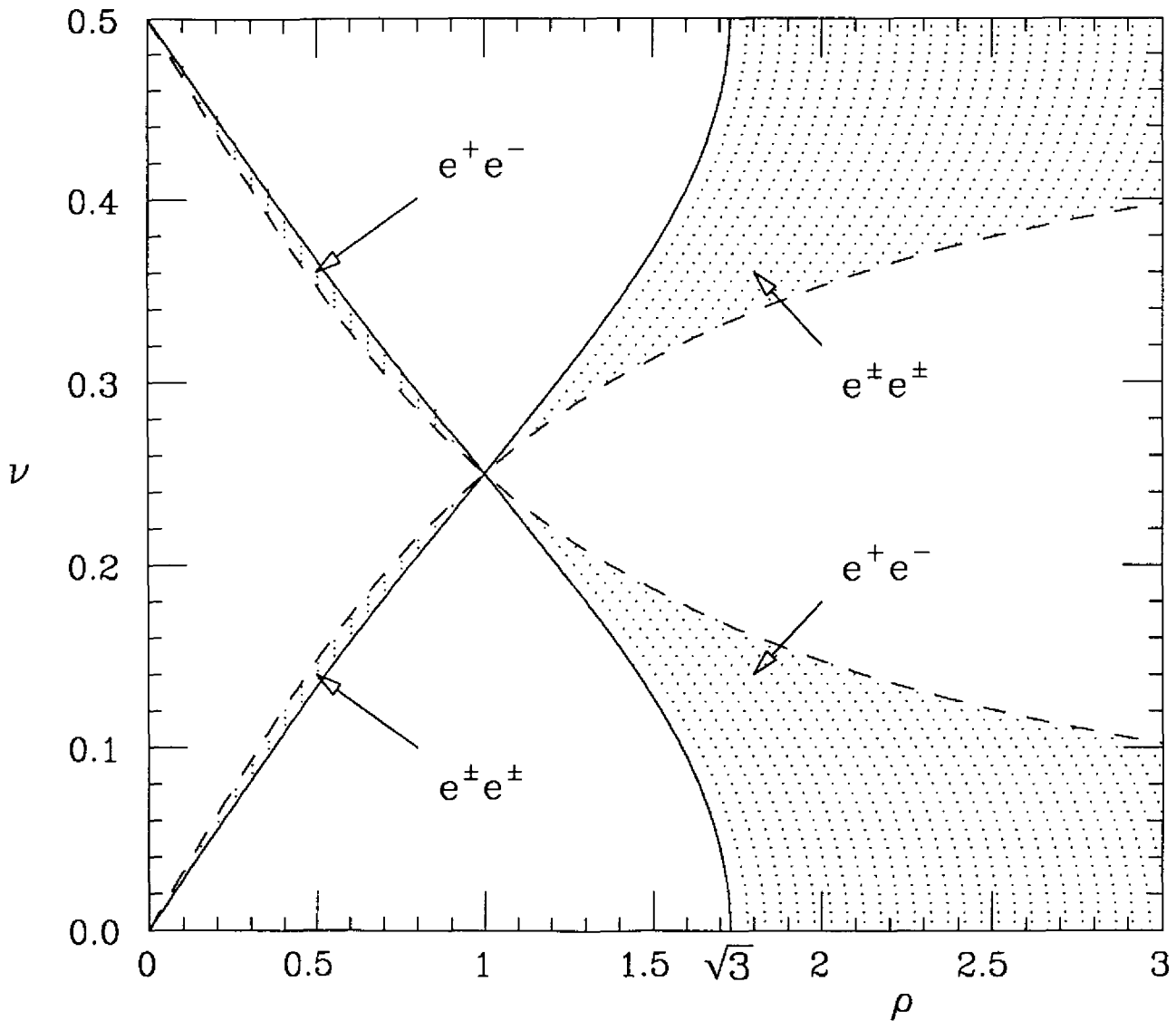

Fig. 1. Regions where the flat–beam, period–1, unequal–size solutions are real (though not necessarily stable).

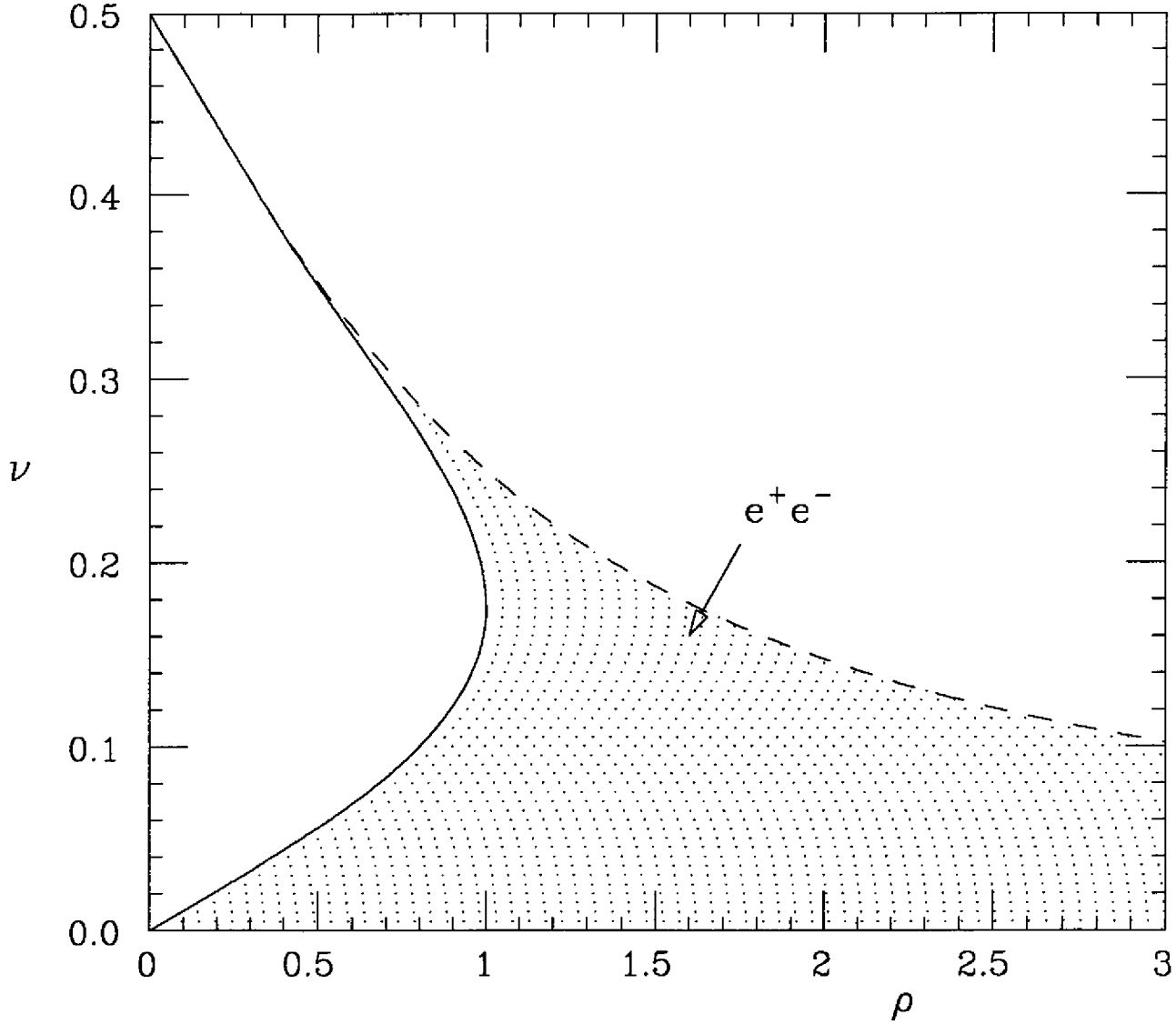

Fig. 2. Region where the round–beam, period–1, unequal–size solutions are real (though not necessarily stable). The $e^{\pm}e^{\pm}$ solutions are always complex.

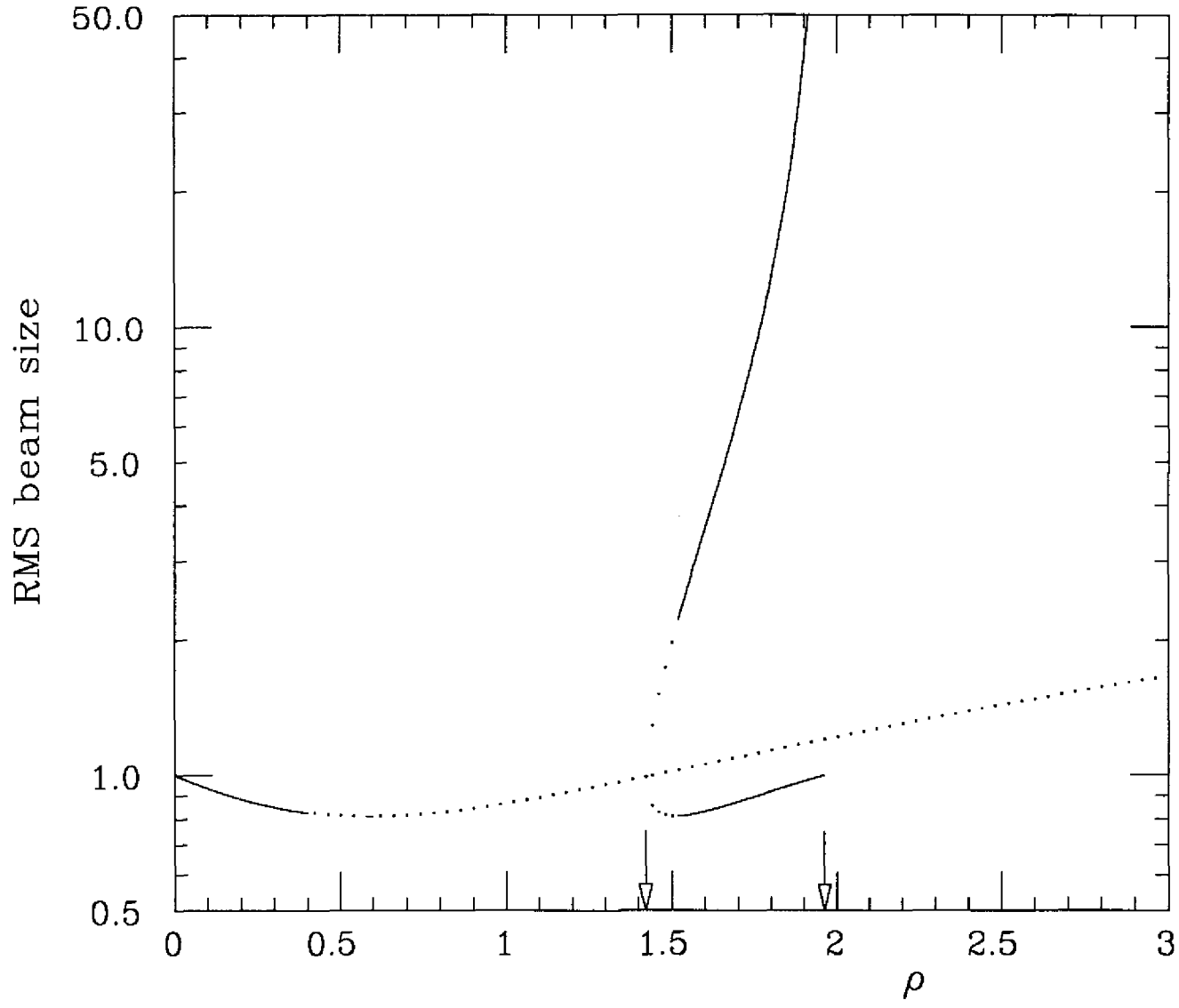

Fig. 3. RMS beam sizes and stability for the period−1 fixed point solutions (solid=stable, dots=unstable). Flat−beam case, ν=0.15, λ=0.8694.

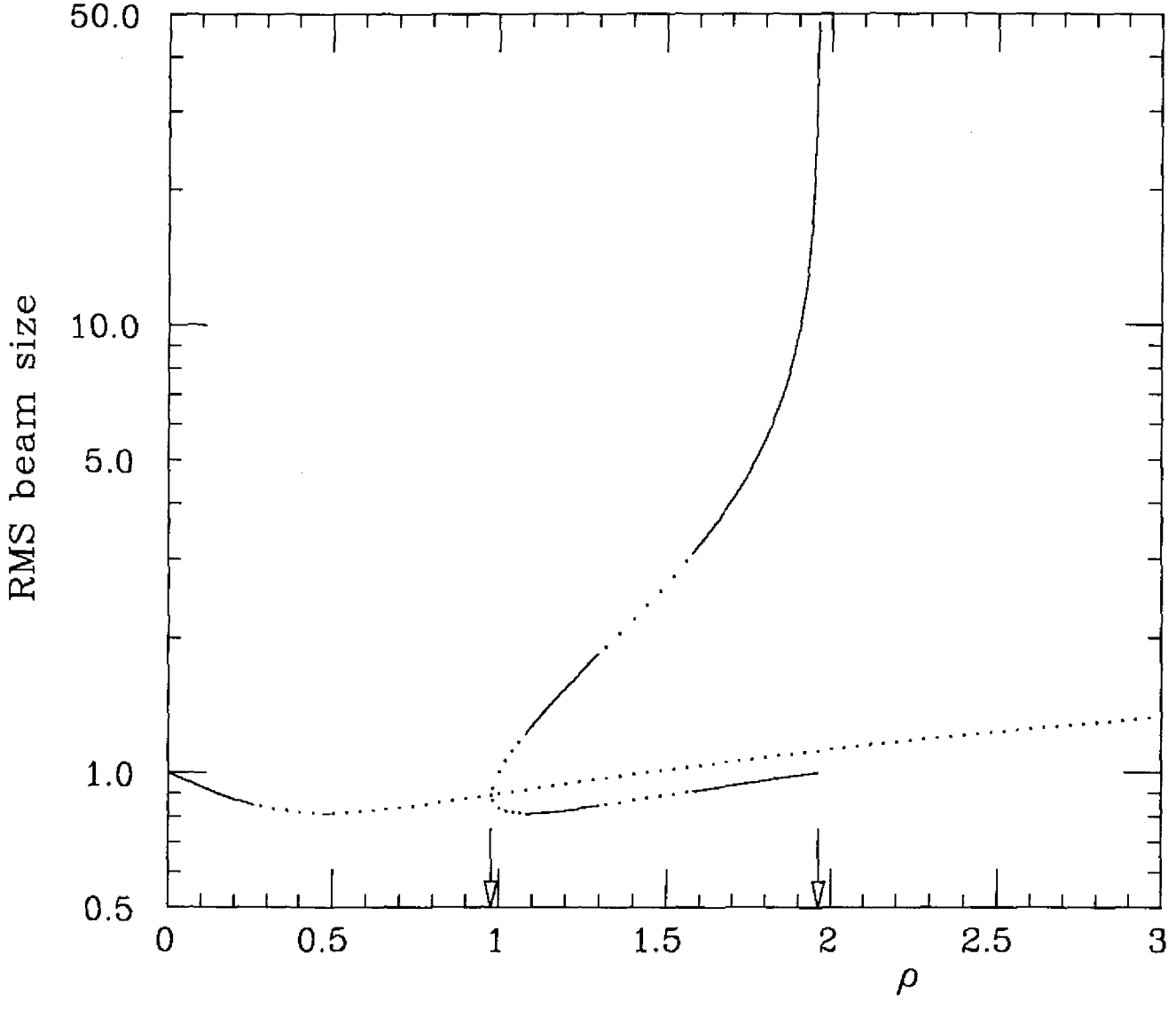

Fig. 4. RMS beam sizes and stability for the period−1 fixed point solutions (solid=stable, dots=unstable). Round−beam case, ν=0.15, λ=0.8694.

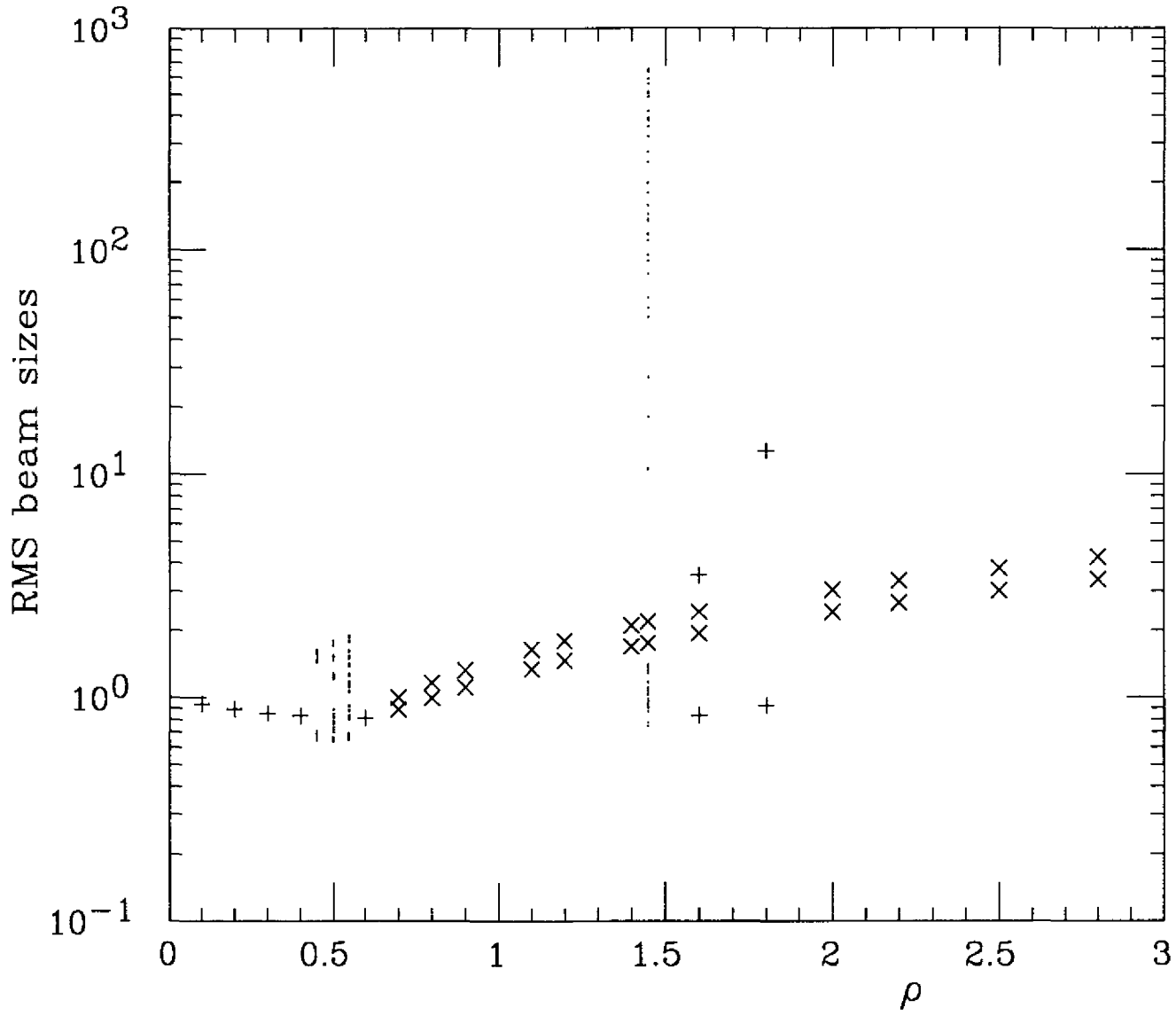

Fig. 5. Flat beam sizes from map iteration; dots=chaotic; +=period−1 (equal or unequal sizes); ×=period−2 (equal sizes). ν=0.15, λ=0.8694.

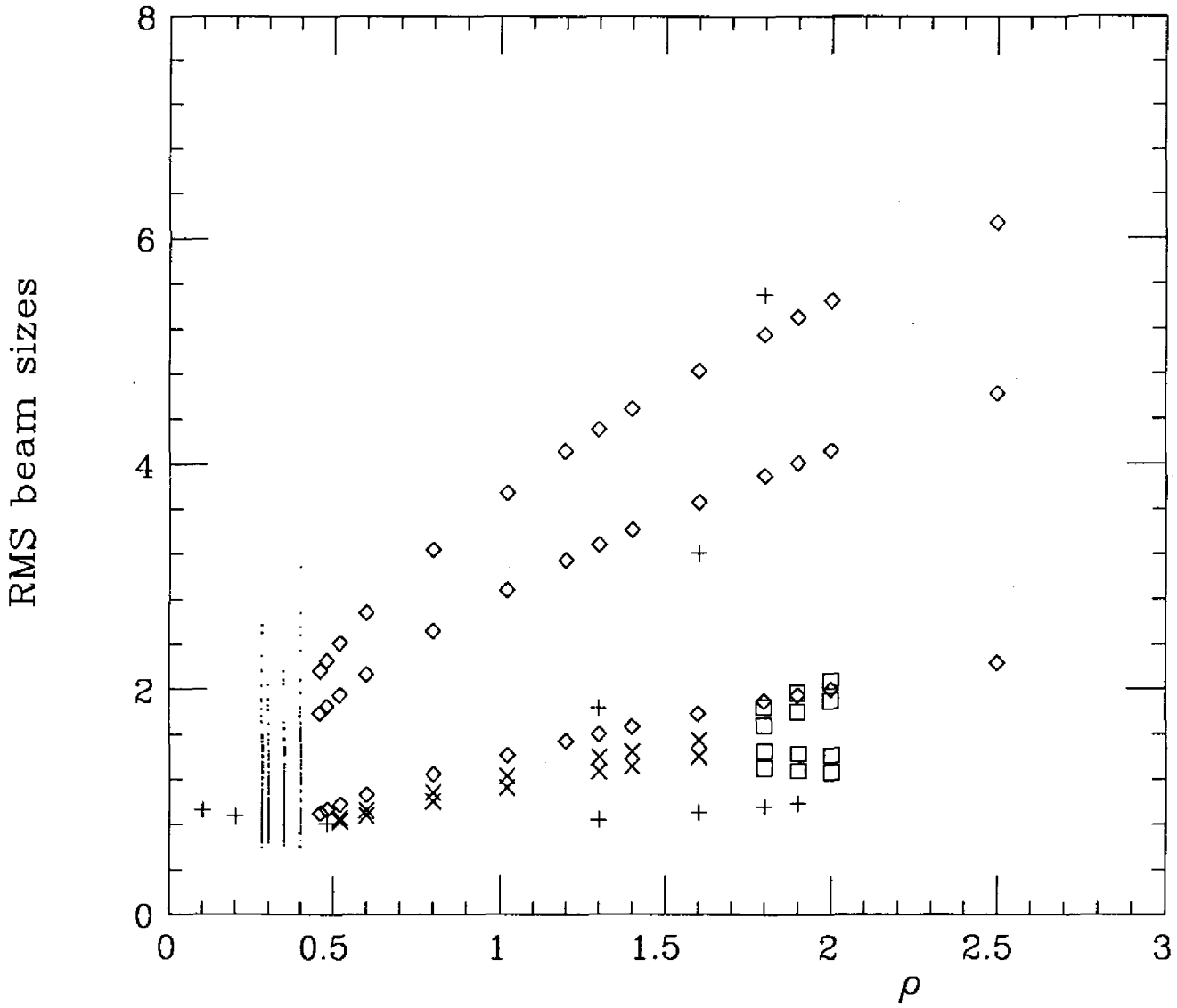

Fig. 6. Round beam sizes from map iteration; dots=chaotic; +=period−1 (equal or unequal sizes); ×=period−2, ◇=period−3, □=period−4 (equal sizes). ν=0.15, λ=0.8694.

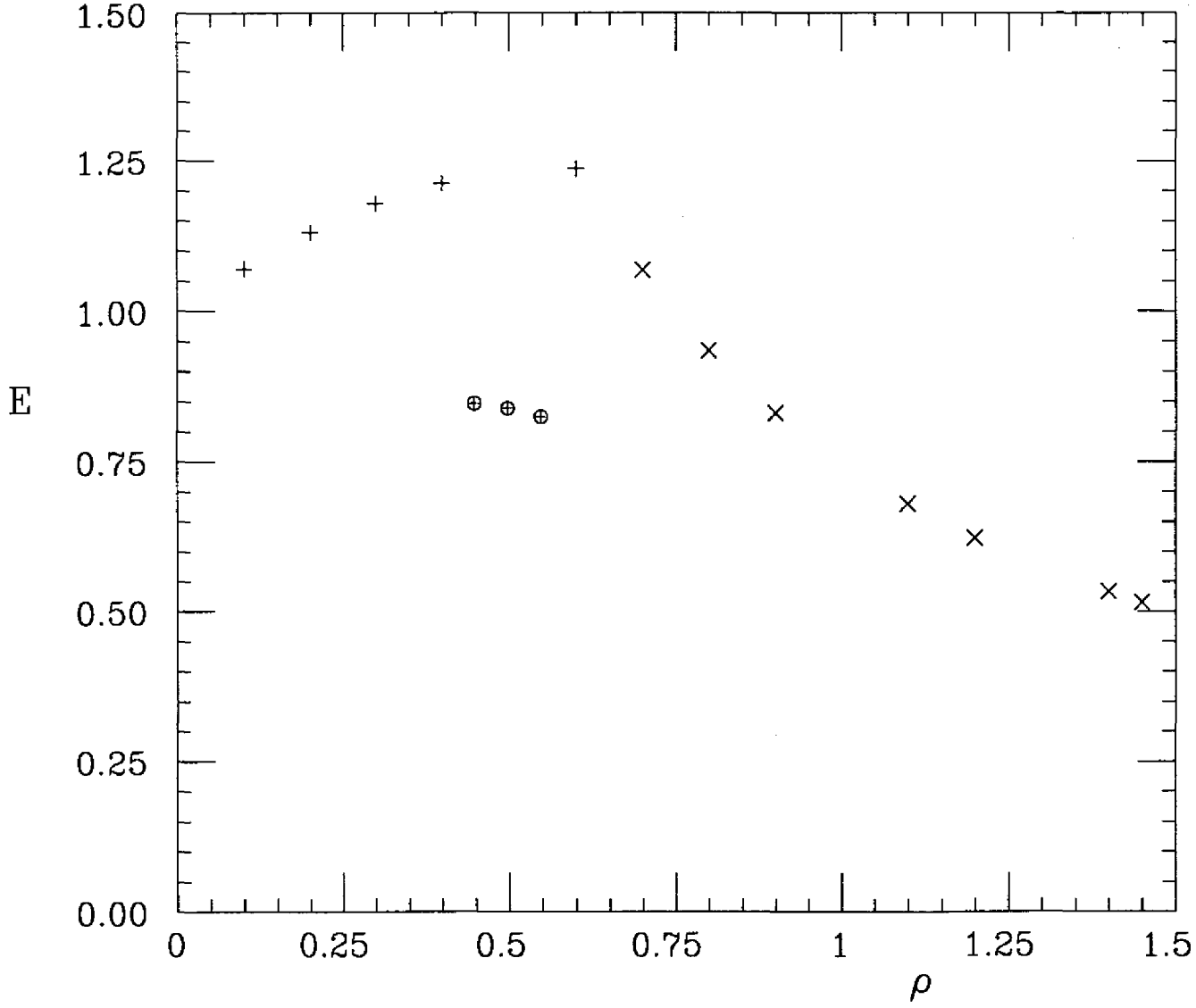

Fig. 7. Flat–beam enhancement factor from period–1 (+), period–2 (×), or chaotic (⊕) fixed points. ν=0.15, λ=0.8694.

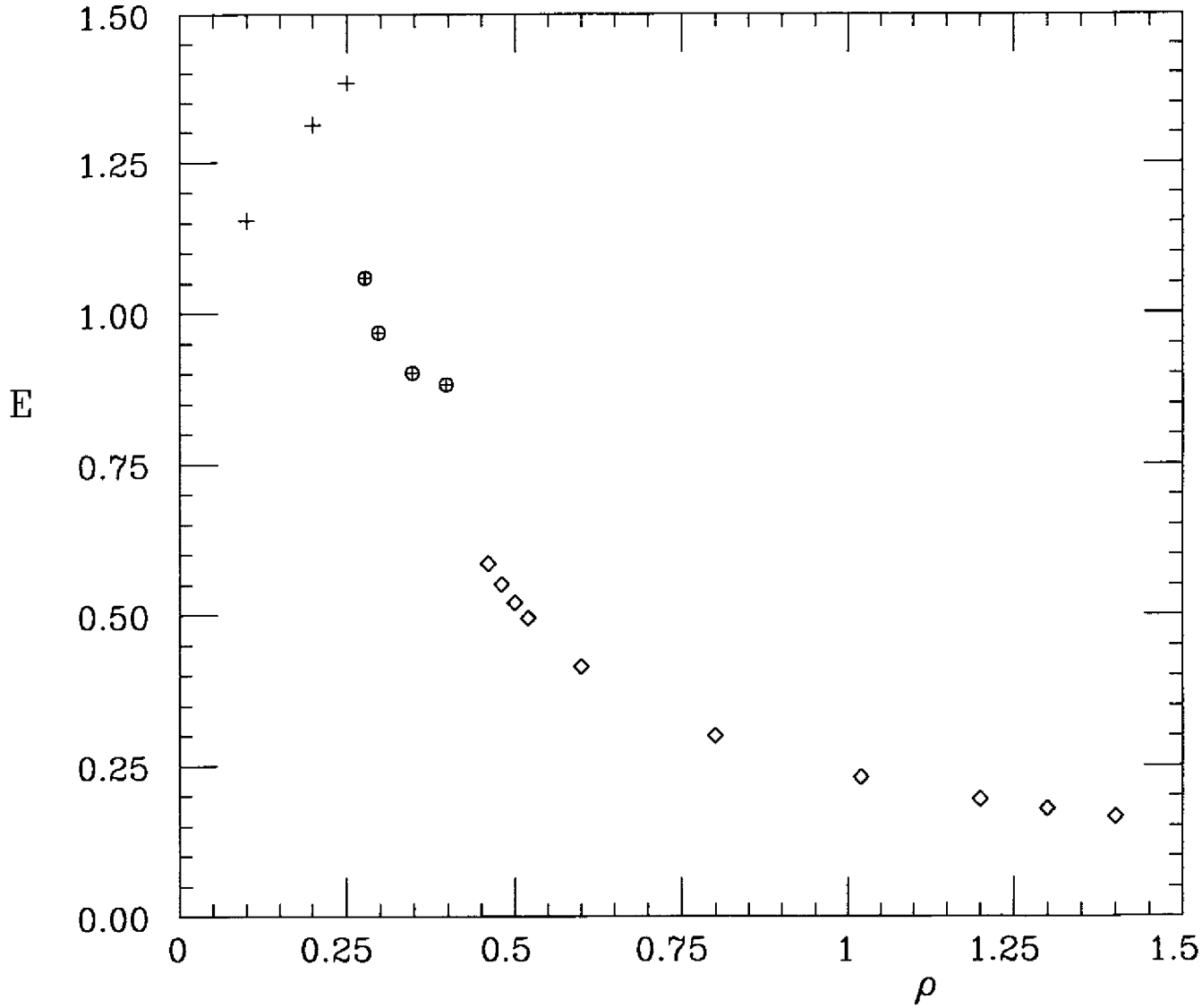

Fig. 8. Round−beam enhancement factor from period−1 (+), period−3 (◇), or chaotic (⊕) fixed points. ν=0.15, λ=0.8694.